# Magnetic Circular Dichroism and Absorption Spectra of the NH Radical in an Argon Matrix

**Vaughan S. Langford and Bryce E. Williamson***

*Department of Chemistry, University of Canterbury, Private Bag 4800, Christchurch, New Zealand*

*Received: December 16, 1997*

Magnetic circular dichroism (MCD) and absorption spectra are reported for the $A\ ^3\Pi \leftarrow X\ ^3\Sigma^-$ transitions of NH and ND in solid Ar over the temperature range 1.6−16 K and the magnetic-field range 0−4.5 T. The data indicate that the guest radicals undergo essentially free rotation in the ground state, but that rotation is strongly hindered in the excited state. The $A\ ^3\Pi$ term is split by spin−orbit coupling (SOC) and crystal-field (CF) interactions. The SOC constants are $A_\Pi(\mathrm{NH/Ar}) = -33.5 \pm 0.3\ \mathrm{cm}^{-1}$ and $A_\Pi(\mathrm{ND/Ar}) = -37.1 \pm 1.0\ \mathrm{cm}^{-1}$. A value of $V_0 \approx 38\ \mathrm{cm}^{-1}$ is determined for the CF parameter. Structure in the spectra is attributed to SO−CF splittings and couplings with librational modes and/or lattice phonons.

## I. Introduction

This paper is the third in a series examining the absorption and magnetic circular dichroism (MCD) spectra of monohydride radicals of first-row elements isolated in Ar matrixes (XH/Ar). The earlier papers concerned OH[1] and CH,[2] which have orbitally degenerate $^2\Pi$ ground states and give MCD spectra dominated by zeroth moment *B*- and *C*-term contributions.[3] The work presented here concerns the $A\ ^3\Pi \leftarrow X\ ^3\Sigma^-$ transition of the NH (imidogen or imine) and ND radicals in Ar. In the absence of ground-state orbital degeneracy, the zeroth MCD moment vanishes, leaving a dominant temperature-dependent first-moment contribution.

$A\ ^3\Pi \leftrightarrow X\ ^3\Sigma^-$ spectra of gas-phase NH were first reported by Eder in 1893.[4] Since then, more precise studies of the emission[5,6] and absorption[6−8] spectra have been analyzed to yield ground- and excited-state parameters,[6,9,10] and have allowed identification of the radical in flames,[11] the interstellar medium,[12] cometary outflows[13,14] and stellar atmospheres.[15,16] Spectra of NH and ND isolated in rare-gas (Ar, Kr, and Xe) matrixes were first reported in 1958 by Robinson and McCarty.[17,18] After further studies,[19] these workers concluded that NH(D) undergoes essentially free rotation in rare-gas lattices. In 1975, Bondybey and Brus reported laser-induced fluorescence for NH(D) in Ar and Kr.[20] They also concluded that the guest radicals undergo essentially free rotation in the ground state, but found that rotations were strongly hindered in the excited state.

There are two previous reports of MCD of matrix-isolated NH. Lund et al. investigated NH/Ar and NH/Xe,[21] but their analysis was hampered by poor resolution and inaccurate thermometry. Rose performed more comprehensive studies on the same systems, and also made a cursory examination of NH/Kr.[22] She found strong and complicated MCD temperature dependence, which she tentatively interpreted to indicate that the guest radicals undergo a transition from orientational disorder at $T \gtrsim 15$ K to complete preferential orientational order along the magnetic-field direction at ∼1.5 K.

The aims of this work are to (i) verify the MCD temperature dependence observed by Rose[22] for the $A\ ^3\Pi \leftarrow X\ ^3\Sigma^-$ system of NH/Ar, (ii) provide a physically realistic model that accounts for the temperature and magnetic-field dependencies of the MCD, and (iii) compare and contrast the results and conclusions for NH/Ar with those obtained earlier for OH/Ar[1,23] and CH/Ar.[2,23]

* Corresponding author. E-mail: B.Williamson@chem.canterbury.ac.nz. Fax: ++ 64 3 364 2110.

## II. Experimental Section

MCD ($\Delta A$) and double-beam absorption ($A$) spectra were measured simultaneously using a spectrometer described elsewhere.[1,23] $\Delta A$ is the difference between the absorbance of left ($A_+$) and right ($A_-$) circularly polarized light by a sample in the presence of a longitudinal magnetic field of inductance $B$, while $A$ is the corresponding average:[3]

$$\Delta A = A_+ - A_- \tag{1}$$

$$A = (A_+ + A_-)/2 \tag{2}$$

$NH_3$ (dry laboratory reagent) or $ND_3$ (Isotec Inc.) was mixed with Ar (1:100 mole ratio) in a 1-L glass reservoir to a final pressure of ∼1 atm. The mixture was allowed to flow at ∼5 mmol $h^{-1}$ through a 4-mm (i.d.) quartz tube, in which it was excited to discharge by a Tesla coil. The products were deposited onto a cryogenically cooled *c*-cut sapphire sample window held at ∼13 K. Deposition times were ∼15 min.

Preliminary experiments were performed by using a closed-cycle He refrigerator (APD Cryogenics) placed between the poles of an Alpha Magnetics 4800 electromagnet.[1,23] These showed that annealing above ∼20 K yielded some band sharpening, but the radical concentration was reduced and the matrix became cloudy. Subsequent experiments were performed without annealing, using an Oxford Instruments SM4 cryomagnet in a matrix injection mode.[24,25] The latter instrument allows stronger magnetic fields, lower temperatures, and more precise thermometry. Spectral resolution was 0.04 nm (∼3.5 $\mathrm{cm}^{-1}$) for NH/Ar and 0.08 nm (∼7 $\mathrm{cm}^{-1}$) for ND/Ar.

## III. Results

Figures 1−4 show the $A\ ^3\Pi \leftarrow X\ ^3\Sigma^-$ MCD and absorption spectra of NH/Ar and ND/Ar at magnetic fields up to 4.5 T and temperatures between 1.6 and 17 K. The spectra for the

S1089-5639(98)00534-9 CCC: $15.00 
Published on Web 03/17/1998

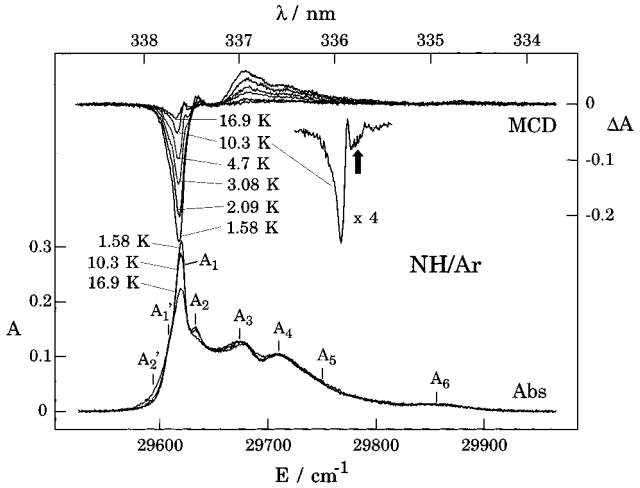


**Figure 1.** Absorption spectrum (*A*; bottom) and temperature dependence of the MCD (Δ*A*; top) for the $A\ ^3\Pi \leftarrow X\ ^3\Sigma^-$ system of NH/Ar ($B = 1$ T). Absorption bands are labeled for cross reference with Table 1. The arrow in the expanded MCD spectrum at $T = 10.3$ K indicates a negative high-temperature *B* term (see text).

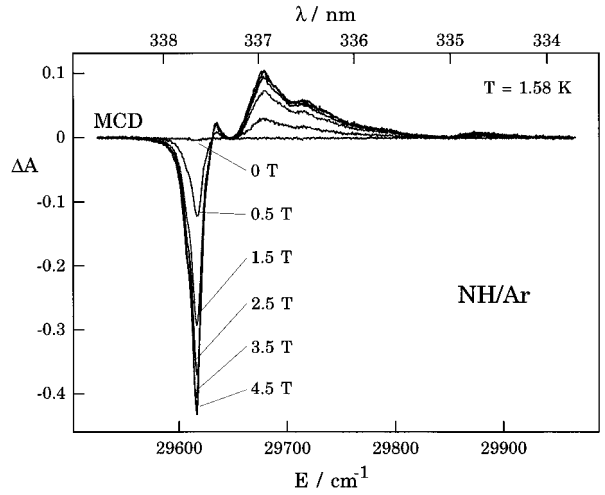


**Figure 2.** MCD magnetic-field dependence for the $A\ ^3\Pi \leftarrow X\ ^3\Sigma^-$ system of NH/Ar at $T = 1.58$ K.

two systems are generally similar, although those for ND/Ar are broader and less structured. The NH/Ar spectra are virtually identical with those reported by Rose.[22]

The absorption spectra are almost temperature independent below ~10 K, but at higher temperatures they exhibit broadening, with hot bands becoming apparent in the case of NH/Ar. The MCD spectra are double-signed, which is generally regarded as a characteristic of *A* terms, but also show the reciprocal temperature dependence indicative of *C* terms.[3] Further evidence for the presence of *C* terms is provided in Figures 2 and 4 by the saturation behavior of the MCD as a function of magnetic field strength; the magnitude of the MCD increases at a progressively slower rate as the field is increased.

The energies of the individual bands observed in the spectra of NH(D)/Ar are listed in Table 1, where they are compared with values obtained by previous workers.[19,22] The sharper bands in the case of NH/Ar allow the identification of more features than for ND/Ar. The shoulder labeled $A_1'$ persists to the lowest temperatures, but its intensity can be reduced by annealing. It is assigned to the presence of a minor metastable site. A shoulder observed at ~29 620 $cm^{-1}$ in the spectra of ND/Ar (arrow in Figure 3) may also indicate a second site, but coincides with band $A_1$ of NH/Ar, to which it is attributed. We

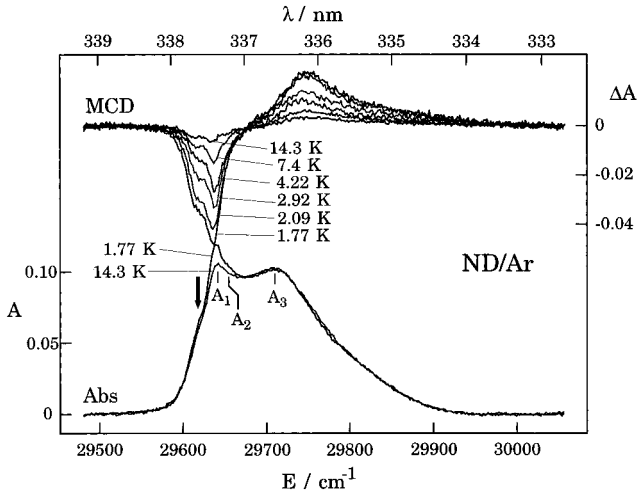


**Figure 3.** Absorption spectrum (*A*; bottom) and temperature dependence of the MCD (Δ*A*; top) for the $A\ ^3\Pi \leftarrow X\ ^3\Sigma^-$ system of ND/Ar ($B = 1$ T). Absorption bands are labeled for cross reference with Table 1. The shoulder near 29 620 $cm^{-1}$ (indicated by an arrow in the absorption spectrum) is attributed to NH/Ar contamination.

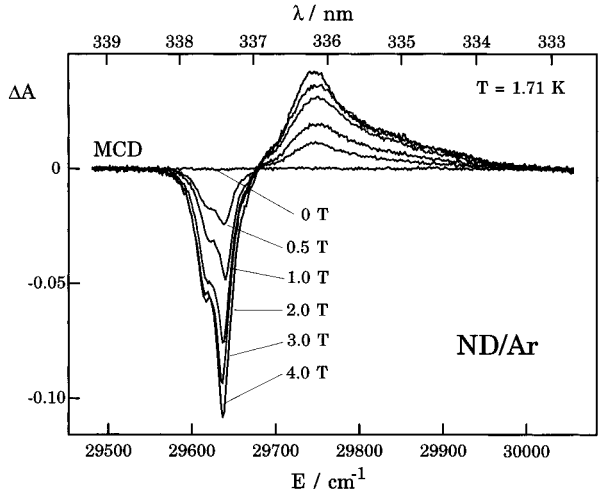


**Figure 4.** MCD magnetic-field dependence for the $A\ ^3\Pi \leftarrow X\ ^3\Sigma^-$ system of ND/Ar at $T = 1.72$ K. The shoulders near 29 620 $cm^{-1}$ is attributed to NH/Ar contamination.

believe that NH is formed due to contamination of the matrix injection apparatus with water, which dissociates in the reaction mixture to produce H atoms. A similar problem was encountered in investigations of CH/Ar.[2,23]

Partial analysis of the spectra is achieved below by using the method of moments.[3] The *n*th absorption ($\mathbf{A}_n$) and MCD ($\mathbf{M}_n$) moments are defined by

$$\mathbf{A}_n = \int \frac{A(E)}{E} (E - \bar{E})^n \, dE \tag{3}$$

$$\mathbf{M}_n = \int \frac{\Delta A(E)}{E} (E - \bar{E})^n \, dE \tag{4}$$

Here $E$ is the photon energy, $\bar{E}$ is the absorption band barycenter (defined by $\mathbf{A}_1 = 0$), and the integrals are carried over the full envelope of the transition. $\mathbf{A}_0$ measures the absorption intensity, and the magnitude of the MCD is quantified by $\mathbf{M}_1$. ($\mathbf{M}_0 = 0$ within experimental error.) The analysis actually employs the ratio $\mathbf{M}_1/\mathbf{A}_0$, which is readily amenable to theoretical interpretation and is independent of poorly known variables such as transition moments and the concentration, path length, and refractive index of the sample.

**TABLE 1: Bands Observed in the $A\ ^3\Pi \leftarrow X\ ^3\Sigma^-$ Systems of NH/Ar and ND/Ar**

| | energy/cm$^{-1}$ | | | | | |
|---|---|---|---|---|---|---|
| | ref 19 | | ref 22 | this work[a] | | |
| band[b] | NH/Ar | ND/Ar | NH/Ar | NH/Ar | ND/Ar[c] | assignments[d] |
| $A_2'$ | | | | 29 595 (−25) | | $^3\Pi_{-}\pm1 \leftarrow {}^3\Sigma^-$ + rot (hot band) |
| $A_1'$ | | | | 29 608 (−12) | | $^3\Pi_{-}\pm1 \leftarrow {}^3\Sigma^-$ (minor site) |
| $A_1$ | 29 581 | 29 608 | 29 551 | 29 620 (0) | 29 642 (0) | $^3\Pi_{-}\pm1 \leftarrow {}^3\Sigma^-$ |
| $A_2$ | 29 597 | | 29 562 | 29 633 (13) | 29 657 (15) | $^3\Pi_{-}0 \leftarrow {}^3\Sigma^-$ |
| $A_3$ | 29 642 | | 29 616 | 29 674 (54) | 29 712 (70) | $^3\Pi_{+}0$, $^3\Pi_{+}\pm1 \leftarrow {}^3\Sigma^-$ |
| $A_4$ | 29 671 | | 29 650 | 29 708 (88) | | $^3\Pi_{+}\pm1 \leftarrow {}^3\Sigma^-$ |
| $A_5$ | | | 29 682 | ∼29 750 (130) | | phonon/libration overtone |
| $A_6$ | | | | 29 853 (233) | | phonon overtone |

[a] Values in parentheses give the displacement from $A_1$. [b] Band labels are shown in Figures 1 and 3. [c] A shoulder at 29 621 cm$^{-1}$ (Figure 3) is attributed to NH/Ar. [d] According to the SO−CF model; see text.

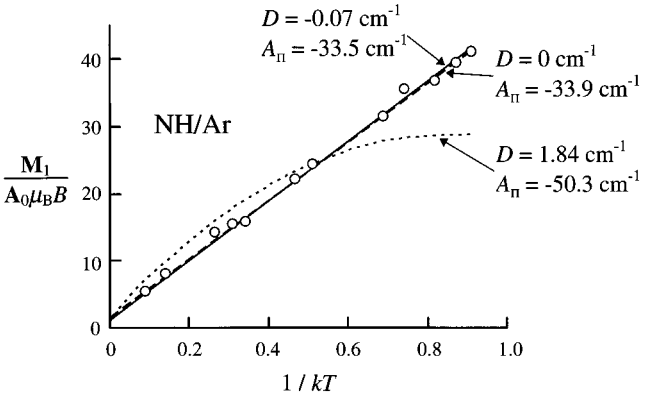


**Figure 5.** Temperature dependence of the ratio $\mathbf{M}_1/(\mathbf{A}_0\mu_B B)$ as a function of $1/kT$ for the $A\ ^3\Pi \leftarrow X\ ^3\Sigma^-$ system of NH/Ar ($\mu_B B \ll kT$). The curves are fits computed using eq 11 with the parameters in Table 3.

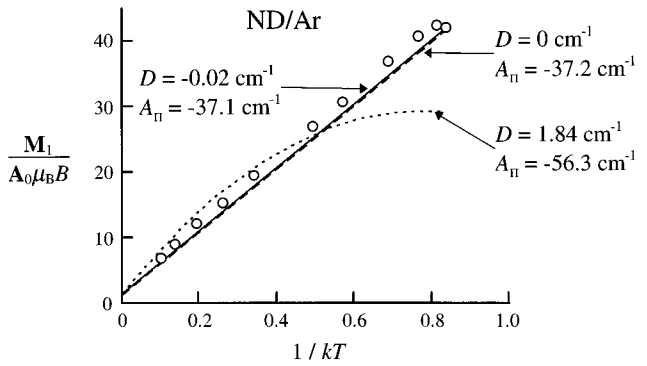


**Figure 6.** Temperature dependence of the ratio $\mathbf{M}_1/(\mathbf{A}_0\mu_B B)$ as a function of $1/kT$ for the $A\ ^3\Pi \leftarrow X\ ^3\Sigma^-$ system of ND/Ar ($\mu_B B \ll kT$). The curves are fits computed using eq 11 with the parameters in Table 3.

Figures 5 and 6 show the dependence of $\mathbf{M}_1/\mathbf{A}_0$ (scaled by $\mu_B B$ where $\mu_B = 0.467$ cm$^{-1}$ T$^{-1}$ is the Bohr magneton) on $1/kT$ ($k = 0.695$ cm$^{-1}$ K$^{-1}$ is Boltzmann's constant). These data were obtained at magnetic field strengths that conform to the linear limit ($\mu_B B \ll kT$),[3] where $\mathbf{M}_1$ is linearly dependent on $B$, and the $C$-term intensity is proportional to $1/T$. MCD saturation data, which extend beyond the linear limit, are shown in Figures 7 and 8.

## IV. Discussion

MCD and its origins are discussed in detail by Piepho and Schatz.[3] In the conventional description, contributions to the MCD are classified as Faraday terms.[3,26] $A$ and $C$ terms are consequences of first-order Zeeman splittings of the initial and/or final levels of a transition. $A$ terms result directly from the Zeeman shifts; they are temperature independent and double-signed with sigmoidal dispersion. $C$ terms are related to ground-state paramagnetism; they are single-signed (either positive or negative) and exhibit a temperature dependence that reflects differences between thermal populations of Zeeman states within the ground-state manifold. Finally, $B$ terms represent diamagnetic contributions arising from magnetic-field-induced mixing of states; they are single-signed and temperature independent.

If the ground-state is degenerate, the MCD is usually dominated by $C$ terms. However, if the degeneracy arises purely from spin, the $C$ terms are only evident if the excited-state levels are split by spin−orbit coupling (SOC); in that case, the MCD comprises pairs of oppositely signed $C$ terms whose separation (due to excited-state SOC) gives the MCD a dispersion that is

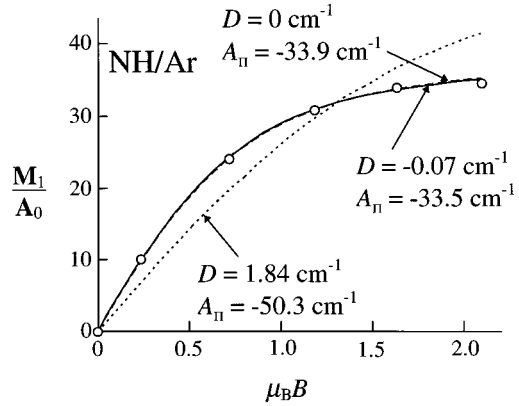


**Figure 7.** Magnetic-field dependence of the ratio $\mathbf{M}_1/\mathbf{A}_0$ as a function of $\mu_B B$ for the $A\ ^3\Pi \leftarrow X\ ^3\Sigma^-$ system of NH/Ar at $T = 1.58$ K. The curves are fits computed using eq 11 with the parameters in Table 3.

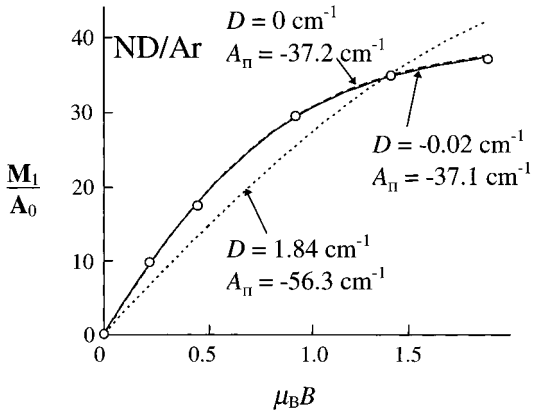


**Figure 8.** Magnetic-field dependence of the ratio $\mathbf{M}_1/\mathbf{A}_0$ as a function of $\mu_B B$ for the $A\ ^3\Pi \leftarrow X\ ^3\Sigma^-$ system of ND/Ar at $T = 1.72$ K. The curves are fits computed using eq 11 with the parameters in Table 3.

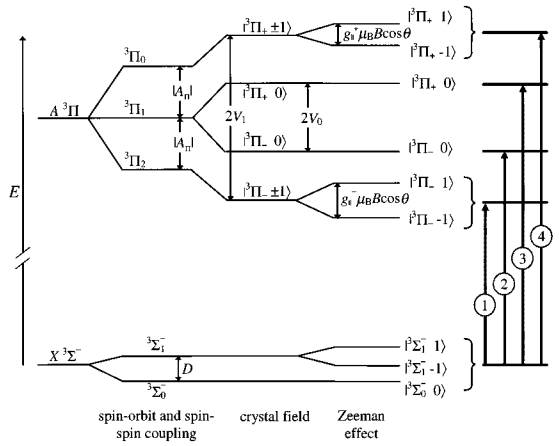


**Figure 9.** Energy-level diagram showing the effects of spin−orbit, spin−spin, crystal-field, and Zeeman interactions on the $X\ ^3\Sigma^-$ and $A\ ^3\Pi$ terms of NH(D)/Ar. Parameter and state notations are given in the text. The arrows on the right-hand side indicate the hypothetical electronic transitions of the SO−CF model.

suggestive of an *A* term, but which shows (reciprocal) temperature dependence. This is exactly the situation for the $A\ ^3\Pi \leftarrow X\ ^3\Sigma^-$ transition of NH(D). In the gas phase, the $A\ ^3\Pi$ term is split by SOC into levels quantized by $\Omega$ (=0, 1, 2; Figure 9), the projection of the total electronic angular momentum on to the internuclear axis. In the following, the corresponding electronic eigenstates are designated $|^3\Pi_\Omega\ M_\Lambda\ \Sigma\rangle$, where $\Sigma = 0, \pm1$ is the projection of the total spin along the internuclear axis and $M_\Lambda = \pm1$ is an orbital partner label defined by $|M_\Lambda + \Sigma| = \Omega$. Note that the states $|^3\Pi_0\ \mp1\ \pm1\rangle$ differ from the conventional $|^3\Pi_{0^\pm}\rangle$,[27] to which they are related by

$$|^3\Pi_0\ \mp1\ \pm1\rangle = (1/2)^{1/2}(|^3\Pi_{0^+}\rangle \pm |^3\Pi_{0^-}\rangle) \tag{5}$$

The $|^3\Pi_0\ \mp1\ \pm1\rangle$ are not mixed by the Zeeman effect and provide a more convenient basis from which to treat crystal-field effects (vide infra). The energies of the $A\ ^3\Pi$ SO levels are

$$E(^3\Pi_\Omega) = T_\Pi + A_\Pi(\Omega - 1) \tag{6}$$

where $T_\Pi$ and $A_\Pi$ are, respectively, the term energy (in the absence of spin) and the SOC constant; $T_\Pi \approx 29\,810$ cm$^{-1}$,[8] while $A_\Pi = -34.79$ cm$^{-1}$ for NH and $-34.58$ cm$^{-1}$ for ND.[9] (The negative $A_\Pi$ values reflect the fact that $A\ ^3\Pi$ is an inverted SO system.) In the presence of a magnetic field, each of these doubly degenerate levels is split by a first-order Zeeman effect that depends on the angle $\theta$ between the magnetic field and the internuclear (*z*) axis of the radical. The Zeeman shifts are

$$E_B(^3\Pi_\Omega M_\Lambda \Sigma) = (M_\Lambda + g_e\Sigma)\,\mu_B B\cos\theta \tag{7}$$

**1. Moment Analysis and Ground-State Zero-Field Splitting.** The states of NH(D) are also susceptible to spin−spin and higher-order SO effects. For the $A\ ^3\Pi$ term, these are small in comparison with $A_\Pi$, and to a good approximation can be neglected. However, for the $X\ ^3\Sigma^-$ term they give rise to a zero-field splitting (ZFS), which is potentially important, especially when the magnitude of the ZFS parameter ($\lambda \approx 0.92$ cm$^{-1}$ for gas-phase NH(D)[28]) is comparable with the thermal energy.

The extent to which ZFS of the $X\ ^3\Sigma^-$ term is *actually* important to the present situation depends critically on the degree to which reorientation of the guest radical is hindered in the matrix. If rotation is suppressed completely, the electronic spin couples to the N−H(D) axis and is quantized by the projections $\Sigma = 0, \pm1$; the corresponding zero-field eigenstates are here designated $|^3\Sigma^-\ \Sigma\rangle$, where $|^3\Sigma^-\ 0\rangle$ is separated from $|^3\Sigma^-\ \pm1\rangle$ by $D = 2\lambda$ (Figure 9).[29] Alternatively, if rotation is completely free, the spin (for a $^3\Sigma$ term) is decoupled from the internuclear axis, and the lowest rotational level (with total angular momentum given by $J = 1$) is triply degenerate in the absence of a magnetic field.[8,27,29] In the latter case, $\Sigma$ is no longer a good quantum number, but the $|^3\Sigma^-\ \Sigma\rangle$ states still constitute a valid basis and can be employed in a general treatment that is independent of the degree of rotational hindrance. This is the approach adopted in the following analysis.

**TABLE 2: Hamiltonian Matrix Elements for the $X\ ^3\Sigma^-$ Term of NH(D)/Ar[a]**

| | $\|^3\Sigma^- -1\rangle$ | $\|^3\Sigma^- 0\rangle$ | $\|^3\Sigma^- 1\rangle$ |
|---|---|---|---|
| $\|^3\Sigma^- -1\rangle$ | $D/3-2Cg_e$ | $\sqrt{2}Sg_e$ | 0 |
| $\|^3\Sigma^- 0\rangle$ | $\sqrt{2}Sg_e$ | $-2D/3$ | $-\sqrt{2}Sg_e$ |
| $\|^3\Sigma^- 1\rangle$ | 0 | $-\sqrt{2}Sg_e$ | $D/3 + 2Cg_e$ |

[a] Basis states are $|^3\Sigma^-\ \Sigma\rangle$; $C = \cos\theta\ \mu_B B/2$; $S = \sin\theta\ \mu_B B/2$.

The effective Hamiltonian matrix for the $X\ ^3\Sigma^-$ term is given in Table 2. *D* is treated as an empirical parameter, with a value that is expected to lie between $\sim 2\lambda$ and zero depending on the degree to which rotation is restricted. The presence of an external magnetic field will mix the basis functions to give Zeeman states of the form

$$|^3\Sigma^-\ i\rangle = \sum_\Sigma C_{\Sigma,i}\,|^3\Sigma^-\ \Sigma\rangle \tag{8}$$

The indices $i = 1, 2, 3$ label the eigenstates in order of ascending energy, and coefficients $C_{\Sigma,i}$ are dependent on *D*, *B*, and $\theta$. State $|^3\Sigma^-\ i\rangle$ has eigenvalue $E_i$ and a Boltzmann weighting

$$P_i = Q^{-1}\exp(-E_i/kT) \tag{9}$$

where *Q* is the electronic partition function:

$$Q = \sum_i \exp(-E_i/kT) \tag{10}$$

In a solid matrix, the $A\ ^3\Pi$ term is also potentially susceptible to lowering of the orbital degeneracy due to crystal-fields (CF) interactions with nearby host atoms. The existence of such effects has been demonstrated previously for diatomic radicals with orbitally degenerate ground states,[1,2,30] for which the magnitude of the CF could be determined by moment analysis. However, lower moments (e.g., $\mathbf{M}_1$ and $\mathbf{A}_0$) obtained by integrating over the entire band system are invariant to unitary transformations on the excited-state basis;[3] hence the data in Figures 5−8 provide no information concerning CF splitting of the $A\ ^3\Pi$ term of NH(D)/Ar. To obtain such information, examination of the structural components (individual bands) of the system is necessary (vide infra). On the other hand, this invariance confers an advantage in allowing theoretical expressions to be derived for $\mathbf{M}_1$ and $\mathbf{A}_0$ without consideration of CF. The result for the ratio $\mathbf{M}_1/\mathbf{A}_0$ is

$$\mathbf{M}_1/\mathbf{A}_0 = \mu_B B - (3A_\Pi/2)\int_{-1}^{1}\sum_{i=1}^{3} P_i\,(|C_{-1,i}|^2 - |C_{+1,i}|^2)\cos\theta\ \mathrm{d}\cos\theta \tag{11}$$

The first term of eq 11 represents the contribution to the MCD

**TABLE 3: Molecular Parameters for the $A\ ^3\Pi \leftarrow X\ ^3\Sigma^-$ Systems of NH/Ar and ND/Ar**

| | $D$/cm$^{-1}$ | $A_\Pi$/cm$^{-1}$ | sum of sq residuals | $V_0$/cm$^{-1}$ | $\kappa$ | $g_{\|\|}{}^+$ | $g_{\|\|}{}^-$ |
|---|---|---|---|---|---|---|---|
| NH (gas phase) | 1.839[a] | −34.79[b] | | | | | |
| | | | NH/Ar | | | | |
| best fit | −0.08 ± 0.03 | −33.5 ± 0.3 | 1.57 | 38 | 0.66 | 2.7 | 5.3 |
| with $D = 0$ | 0 (fixed) | −33.9 ± 0.5 | 1.66 | | | | |
| with gas-phase $D$ | 1.84 (fixed) | −50.3 ± 6.4 | 131 | | | | |
| ND (gas phase) | 1.837[a] | −34.58[b] | | | | | |
| | | | ND/Ar | | | | |
| best fit | −0.02 ± 0.06 | −37.1 ± 1.0 | 3.20 | 38 | 0.70 | 2.6 | 5.4 |
| with $D = 0$ | 0 (fixed) | −37.2 ± 1.0 | 3.20 | | | | |
| with gas-phase $D$ | 1.84 (fixed) | −56.3 ± 7.2 | 97 | | | | |

[a] Reference 28. [b] Reference 9.

from the excited-state orbital angular momentum, while the second represents the contribution due to excited-state SOC. (In the absence of an excited-state CF, these are respectively associated with conventional $A$ and $C$ terms. In the presence of a CF, both contain $B$-term contributions.) The integral over cos $\theta$ accounts for random orientation of the guest radicals.

Equation 11 depends on $A_\Pi$ and $D$, experimental values for which were determined by nonlinear least-squares fitting of the moment ratios in Figures 5−8. For each isotopomer the data were treated as a surface defined by $\mu_B B$, $1/kT$, and dependent variable $\mathbf{M}_1/\mathbf{A}_0$. Integrals over cos $\theta$ and the necessary derivatives were evaluated numerically. The results are plotted on the appropriate figures and the corresponding parameter values are summarized in Table 3. Fits obtained by constraining $D = 2\lambda \approx 1.84$ cm$^{-1}$ (i.e., assuming nonrotating radicals) are very poor and yield unreasonably large values for $A_\Pi$. With $D$ unconstrained, vastly superior results are obtained where $A_\Pi$ lies within a few percent of the gas-phase values and $D$ is reduced essentially to zero. Fits obtained with $D$ constrained exactly to zero are only marginally inferior. Thus we conclude, in agreement with McCarty and Robinson[19] and Bondybey and Brus,[20] that $X\ ^3\Sigma^-$ NH(D) in Ar behaves essentially as a free rotor.

With $D = 0$, eq 11 can be rewritten in a simpler form that allows the data in Figures 5−8 to be rationalized. Analytical eigenvalues and eigenfunctions of Table 2 permit the integrand of eq 11 to be reduced to

$$\sum_{i=1}^{3} P_i \left(|C_{-1,i}|^2 - |C_{+1,i}|^2\right) \cos\theta = (P_1 - P_3)\cos^2\theta \quad (D = 0) \tag{12}$$

Here $P_1$ and $P_3$ are respectively the populations of the lowest- and highest-energy Zeeman states of the ground-state $J = 1$ manifold; they are independent of $\theta$ and are obtained by substituting $E_i = (i - 2)g_e\mu_B B$ into eq 9. Combining eqs 11 and 12, then averaging over $\theta$, gives

$$\mathbf{M}_1/\mathbf{A}_0 = \mu_B B - A_\Pi(P_1 - P_3) \quad (D = 0)$$

$$= \mu_B B - 2A_\Pi \sinh(g_e\mu_B B/kT)/(1 + 2\cosh(g_e\mu_B B/kT)) \quad (D = 0) \tag{13}$$

In the low-field ($\mu_B B \ll kT$) limit, this simplifies to

$$\mathbf{M}_1/\mathbf{A}_0 \approx \mu_B B(1 - 2g_e A_\Pi/3kT) \quad (D = 0; \mu_B B \ll kT) \tag{14}$$

Hence, in Figures 5 and 6, $\mathbf{M}_1/\mathbf{A}_0\mu_B B$ exhibits approximately linear dependence on $1/kT$, with a slope determined by $A_\Pi$ and an ordinate intercept of 1. At high fields

$$\mathbf{M}_1/\mathbf{A}_0 \approx \mu_B B - A_\Pi \quad (D = 0; \mu_B B \gg kT) \tag{15}$$

So the data in Figures 7 and 8 ($\mathbf{M}_1/\mathbf{A}_0$ against $\mu_B B$) approach linear asymptotes at both low (eq 14) and high fields (eq 15).

**2. Excited-State Crystal-Field Effects.** Having established that $X\ ^3\Sigma^-$ NH(D) behaves essentially as a free rotor in solid Ar, the question arises as to whether these radicals undergo free rotation in their $A\ ^3\Pi$ states. This was the conclusion initially reached by McCarty and Robinson[19] on the basis of correlations with gas-phase transition energies. However, the resulting assignments would require the transition intensity to be concentrated in bands $A_1$ and $A_2$,[8] in contradiction to experiment. Bondybey and Brus later concluded that NH(D) in its $A\ ^3\Pi$ term deviates strongly from a free rotor in Ar.[20] In the following we assume the latter, in which case the excited-state radical should be subject to CF interactions of the type elucidated previously for TiO/Ar,[30] OH/Ar,[1,23] and CH/Ar.[2,23]

The SO−CF Hamiltonian matrix for the $A\ ^3\Pi$ term is constructed (in the SO basis) by augmenting the diagonal elements of eq 6 with off-diagonal CF elements

$$\langle {}^3\Pi_\Omega\, M_\Lambda\, \Sigma | H_{CF} |\, {}^3\Pi_{\Omega'}\, M'_\Lambda\, \Sigma' \rangle = (-1)^{\Omega+1} V_0\, \delta_{M_\Lambda, M'_\Lambda \pm 1}\, \delta_{\Sigma,\Sigma'} \tag{11}$$

where $V_0$ measures the strength of the CF. The matrix factors into three $2 \times 2$ blocks, according to the value of $\Sigma$. The eigenfunctions for each block are denoted $|{}^3\Pi_\pm\, \Sigma\rangle$, where the ${}^3\Pi_+$ states lie at higher energy (Figure 9). The SO−CF energies (excluding the common term value $T_\Pi$) are:

$$E({}^3\Pi_\pm \Sigma) = \pm(A_\Pi{}^2\, |\Sigma| + V_0{}^2)^{1/2} \equiv \pm V_{|\Sigma|} \tag{12}$$

The corresponding eigenstates are:

$$|{}^3\Pi_\pm\, 0\rangle = (1/2)^{1/2}(|{}^3\Pi_1\, 1\, 0\rangle \pm |{}^3\Pi_1\, -1\, 0\rangle) \tag{13}$$

$$|{}^3\Pi_+\, \pm 1\rangle = \alpha\, |{}^3\Pi_0\, \mp 1\, \pm 1\rangle - \beta\, |{}^3\Pi_2\, \pm 1\, \pm 1\rangle \tag{14}$$

$$|{}^3\Pi_-\, \pm 1\rangle = \beta\, |{}^3\Pi_0\, \mp 1\, \pm 1\rangle + \alpha\, |{}^3\Pi_2\, \pm 1\, \pm 1\rangle \tag{15}$$

where the mixing coefficients are

$$\alpha = V_0/[V_0{}^2 + (V_1 + A_\Pi)^2]^{1/2} \tag{16}$$

$$\beta = V_0/[V_0{}^2 + (V_1 - A_\Pi)^2]^{1/2} \tag{17}$$

Zeeman matrix elements for these states are listed in Table 4; the operator is $-\mu_Z B = (L_Z + g_e S_Z)\mu_B B$, where $Z$ designates the magnetic-field axis in the laboratory reference frame. The $g$ values and parameters $\kappa$ and $\eta$ are defined by

**TABLE 4: Zeeman Matrix Elements for the *A* $^3\Pi$ SO−CF States of NH(D)/Ar[a]**

| $-\mu_Z B$ | $\|^3\Pi_- -1\rangle$ | $\|^3\Pi_- 1\rangle$ | $\|^3\Pi_- 0\rangle$ | $\|^3\Pi_+ 0\rangle$ | $\|^3\Pi_+ -1\rangle$ | $\|^3\Pi_+ 1\rangle$ |
|---|---|---|---|---|---|---|
| $\langle^3\Pi_- -1\|$ | $-Cg_{\|\|}-$ | 0 | $Sg_e(\alpha+\beta)$ | $-Sg_e(\alpha-\beta)$ | $2C\eta$ | 0 |
| $\langle^3\Pi_- 1\|$ | 0 | $Cg_{\|\|}-$ | $Sg_e(\alpha+\beta)$ | $Sg_e(\alpha-\beta)$ | 0 | $-2C\eta$ |
| $\langle^3\Pi_- 0\|$ | $Sg_e(\alpha+\beta)$ | $Sg_e(\alpha+\beta)$ | 0 | $2C$ | $Sg_e(\alpha-\beta)$ | $Sg_e(\alpha-\beta)$ |
| $\langle^3\Pi_+ 0\|$ | $-Sg_e(\alpha-\beta)$ | $Sg_e(\alpha-\beta)$ | $2C$ | 0 | $Sg_e(\alpha+\beta)$ | $-Sg_e(\alpha+\beta)$ |
| $\langle^3\Pi_+ -1\|$ | $2C\eta$ | 0 | $Sg_e(\alpha-\beta)$ | $Sg_e(\alpha+\beta)$ | $-Cg_{\|\|}+$ | 0 |
| $\langle^3\Pi_+ 1\|$ | 0 | $-2C\eta$ | $Sg_e(\alpha-\beta)$ | $-Sg_e(\alpha+\beta)$ | 0 | $Cg_{\|\|}+$ |

[a] $C = \cos\theta\ \mu_B B/2$; $S = \sin\theta\ \mu_B B/2$; $g_{\|\|}^+$ and $g_{\|\|}^-$ are defined by eq 18; $\eta$ is defined by eq 20.

$$g_{\|\|}^{\pm} = 2(g_e \mp \kappa) \tag{18}$$

$$\kappa = \alpha^2 - \beta^2 = -A_\Pi/V_1 \tag{19}$$

$$\eta = 2\alpha\beta = V_0/V_1 \tag{20}$$

$\kappa$ represents the CF quenching of the orbital contribution to $g_{\|\|}^{\pm}$, and is referred to as the orbital reduction factor.

The remaining information required to derive expressions for the absorption and MCD moments involves the electric dipole transition moments. Those for $|^3\Pi_\pm\Sigma\rangle \leftarrow |^3\Sigma^-\Sigma\rangle$ obey the selection rule $\Delta\Sigma = 0$, and are given in Table 5; $m_{\pm1}$ are circularly polarized components of the electric dipole moment operator in the molecular (*x*, *y*, z) reference frame:

$$m_{\pm1} = \mp(2)^{-1/2}(m_x \pm i m_y) \tag{21}$$

and $M$ is the one-electron reduced transition moment for the excitation $1\pi \leftarrow 3\sigma$

$$M = \langle 1\pi||m||3\sigma\rangle \tag{22}$$

The transition moments and intensities for $|^3\Pi_\pm\Sigma\rangle \leftarrow |^3\Sigma^- i\rangle$ are obtained from Table 5 by application of eq 8. Transformation from laboratory to molecule-fixed coordinates[1] utilizes the fact that $^3\Pi \leftarrow {}^3\Sigma^-$ transitions are *x*, *y* polarized.

Absorbance measures the average intensity of the left and right circularly polarized transitions (eq 2). Hence, for a molecule whose *z* axis makes angle $\theta$ with respect to the magnetic field,

$$\mathbf{A}_0{}^\theta(^3\Pi_\pm\,\Sigma \leftarrow {}^3\Sigma^-\,i) = (\gamma/4)(1+\cos^2\theta)P_i|C_{\Sigma,i}|^2\,(|\langle^3\Pi_\pm\,\Sigma\,|m_{+1}|^3\Sigma^-\,\Sigma\rangle|^2 + |\langle^3\Pi_\pm\,\Sigma\,|m_{-1}|^3\Sigma^-\,\Sigma\rangle|^2) \tag{23}$$

The coefficient $\gamma$ contains a number of constants, including refractive index corrections and the concentration and path length of the sample. The corresponding MCD intensity comprises *B*- and *C*-term contributions, $\mathbf{C}_0{}^\theta$ and $\mathbf{B}_0{}^\theta$:

$$\mathbf{M}_0{}^\theta(^3\Pi_\pm\,\Sigma \leftarrow {}^3\Sigma^-\,i) = \mathbf{B}_0{}^\theta(^3\Pi_\pm\,\Sigma \leftarrow {}^3\Sigma^-\,i) + \mathbf{C}_0{}^\theta(^3\Pi_\pm\,\Sigma \leftarrow {}^3\Sigma^-\,i) \tag{24}$$

$\mathbf{C}_0{}^\theta$ is simply the difference between left and right circularly polarized intensities

$$\mathrm{C}_0{}^\theta(^3\Pi_\pm\,\Sigma \leftarrow {}^3\Sigma^-\,i) = \gamma\cos\theta\,P_i|C_{\Sigma,i}|^2\,(|\langle^3\Pi_\pm\,\Sigma\,|m_{+1}|^3\Sigma^-\,\Sigma\rangle|^2 - |\langle^3\Pi_\pm\,\Sigma\,|m_{-1}|^3\Sigma^-\Sigma\rangle|^2) \tag{25}$$

$\mathbf{B}_0{}^\theta$ is treated by first-order perturbation theory, assuming that the only significant magnetic-field-induced interactions involve intraterm coupling within the *A* $^3\Pi$ manifold. (Effects of ground-state coupling are contained in the coefficients $C_{\Sigma,i}$.) Using $\sigma = \pm$ to designate the upper and lower excited-state SO−CF levels, the result is

**TABLE 5: Transition Moments for $|^3\mathbf{\Pi}_\pm\,\mathbf{\Sigma}\rangle \leftarrow |^3\mathbf{\Sigma}^-\,\mathbf{\Sigma}\rangle$ of NH(D)/Ar[a]**

| $m_{\pm1}$ | $\|^3\Sigma^- -1\rangle$ | $\|^3\Sigma^- 0\rangle$ | $\|^3\Sigma^- 1\rangle$ |
|---|---|---|---|
| $\langle^3\Pi_\mp -1\|$ | $\beta M/\sqrt{2}$ | 0 | 0 |
| $\langle^3\Pi_\mp 0\|$ | 0 | $M/2$ | |
| $\langle^3\Pi_\mp 1\|$ | 0 | 0 | $\mp\alpha M/\sqrt{2}$ |
| $\langle^3\Pi_\pm -1\|$ | $\pm\alpha M/\sqrt{2}$ | 0 | 0 |
| $\langle^3\Pi_\pm 0\|$ | 0 | $\pm M/2$ | 0 |
| $\cdot^3\Pi_\pm 1\|$ | 0 | 0 | $\beta M/\sqrt{2}$ |

[a] $m_{\pm1}$ is defined by eq 21; $M$ is defined by eq 22.

$$\mathbf{B}_0{}^\theta(^3\Pi_\sigma\,\Sigma \leftarrow {}^3\Sigma^-\,i) = -2\gamma\cos\theta\,P_i\,Re\sum_{\sigma',\Sigma'\neq\sigma,\Sigma}\frac{\langle^3\Pi_{\sigma'}\,\Sigma'|-\mu_Z B|^3\Pi_\sigma\,\Sigma\rangle}{E(^3\Pi_{\sigma'}\,\Sigma') - E(^3\Pi_\sigma\,\Sigma)}\times C_{\Sigma',i}C^*_{\Sigma,i}(\langle^3\Pi_{\sigma'}\,\Sigma'|m_{+1}|^3\Sigma^-\,'\rangle\,\langle^3\Pi_\sigma\,\Sigma|m_{+1}|^3\Sigma^-\,\Sigma\rangle^* - \langle^3\Pi_{\sigma'}\,\Sigma'|m_{-1}|^3\Sigma^-\,\Sigma'\rangle\,\langle^3\Pi_\sigma\,\Sigma|m_{-1}|^3\Sigma^-\,\Sigma\rangle^*) \tag{26}$$

Here, *Re* indicates the real part of everything to the right. The required Zeeman matrix elements are the off diagonals of Table 4, and the energies are given by eq 12.

Moment expressions for individual transitions are given in Table 6. The bottom row gives the sums (obtained using $\sum_i P_i = 1$ and $\sum_i |C_{\Sigma,i}|^2 = \sum_\Sigma |C_{\Sigma,i}|^2 = 1$) over all initial and final states. It is seen that these sums are independent of both ground-state ZFS and excited-state CF, and yield $\mathbf{M}_0 = 0$, in agreement with the experimental result. Determination of the overall $\mathbf{M}_1$ requires that consistency be maintained in the order of perturbation theory. The result is

$$\mathbf{M}_1{}^\theta = \sum_{\sigma,\Sigma,i}[\mathbf{C}_0{}^\theta(^3\Pi_\sigma\Sigma \leftarrow {}^3\Sigma^-i)\Delta E_B(^3\Pi_\sigma\Sigma \leftarrow {}^3\Sigma^-i) + \mathbf{B}_0{}^\theta(^3\Pi_\sigma\Sigma \leftarrow {}^3\Sigma^-i)\Delta E_0(^3\Pi_\sigma\Sigma \leftarrow {}^3\Sigma^-i)] \tag{27}$$

where $\Delta E_B$ and $\Delta E_0$ are, respectively, the transition energies in the presence and absence of a magnetic field. After summing the various contributions and averaging over $\theta$, $\mathbf{M}_1/\mathbf{A}_0$ for the entire system is (as anticipated) given by eq 11, which is independent of CF parameters. Hence, as stated above, the data in Figures 5−8 yield no information concerning excited-state CF effects. However, the magnitude of the CF can, in principle, be estimated by consideration of structure observed in the spectra, since the transition energies and the individual MCD moments of Table 6 *are* dependent on $V_0$. This objective is substantially facilitated by having established that $D = 0$, which allows the expressions of Table 6 to be reduced to analytical form. In the following we perform such an analysis, concentrating initially on NH/Ar since the broader bands in ND/Ar

**TABLE 6: Moment Expressions for Individual $|^3\Pi_\pm\ \Sigma\rangle \leftarrow |^3\Sigma^-\ i\rangle$ Transitions of NH(D)/Ar**

| transition | $\mathbf{A}_0{}^{\theta\ a}$ | $\mathbf{C}_0{}^{\theta\ b}$ | $\mathbf{B}_0{}^{\theta\ b}$ |
|---|---|---|---|
| $\lvert^3\Pi_+ \pm1\rangle \leftarrow \lvert^3\Sigma^- i\rangle$ | $K_A P_i \lvert C_{\pm1,i}\rvert^2$ | $\mp K_M\kappa P_i \lvert C_{\pm1,i}\rvert^2$ | $-K_M\mu_B B P_i\left[\frac{\sqrt{2}g_e \sin\theta}{A_\Pi}C_{\pm1,i}C^*_{0,i} - \frac{\cos\theta\,\eta^2}{V_1}\lvert C_{\pm1,i}\rvert^2\right]$ |
| $\lvert^3\Pi_\pm 0\rangle \leftarrow \lvert^3\Sigma^- i\rangle$ | $K_A P_i \lvert C_{0,i}\rvert^2$ | 0 | $K_M\mu_B B P_i\left[\frac{\sqrt{2}g_e \sin\theta}{A_\Pi}(C_{0,i}C^*_{+1,i} + C^*_{-1,i}) \pm \frac{\cos\theta}{V_0}\lvert C_{0,i}\rvert^2\right]$ |
| $\lvert^3\Pi_- \pm1\rangle \leftarrow \lvert^3\Sigma^- i\rangle$ | $K_A P_i \lvert C_{\pm1,i}\rvert^2$ | $\pm K_M\kappa P_i \lvert C_{\pm1,i}\rvert^2$ | $-K_M\mu_B B P_i\left[\frac{\sqrt{2}g_e \sin\theta}{A_\Pi}C_{\pm1,i}C^*_{0,i} + \frac{\cos\theta\,\eta^2}{V_1}\lvert C_{\pm1,i}\rvert^2\right]$ |
| $A\ ^3\Pi \leftarrow X\ ^3\Sigma^-$ | $2K_A$ | 0 | 0 |

[a] $K_A = \gamma|M|^2(1 + \cos^2\theta)/8$. [b] $K_M = \gamma|M|^2\cos\theta/2$.

**TABLE 7: Moment Expressions for SO−CF Bands of the $A\ ^3\Pi \leftarrow X\ ^3\Sigma^-$ System of NH(D)/Ar Assuming $D = 0$[a]**

| band | excited state(s) | $\mathbf{A}_0$ | $\mathbf{C}_0$ | $\mathbf{B}_0$ | $\mathbf{M}_1$ |
|---|---|---|---|---|---|
| 4 | $\lvert^3\Pi_+ \pm1\rangle$ | $\gamma'(7 - P_2)/60$ | $\gamma'\kappa(P_1 - P_3)/6$ | $(\gamma'/15)\mu_B B\left[\frac{g_e}{A_\Pi}(1 - 3P_2) + \frac{\eta^2}{V_1}(2 - P_2)\right]$ | $(\gamma'\kappa/30)\mu_B B[\kappa(4 - P_2) + g_e(1 - 3P_2)]$ |
| 3 | $\lvert^3\Pi_+ 0\rangle$ | $\gamma'(3 + P_2)/60$ | 0 | $-(\gamma'/15)\mu_B B\left[\frac{g_e}{A_\Pi}(1 - 3P_2) - \frac{1}{2V_0}(1 + 2P_2)\right]$ | 0 |
| 2 | $\lvert^3\Pi_- 0\rangle$ | $\gamma'(3 + P_2)/60$ | 0 | $-(\gamma'/15)\mu_B B\left[\frac{g_e}{A_\Pi}(1 - 3P_2) + \frac{1}{2V_0}(1 + 2P_2)\right]$ | 0 |
| 1 | $\lvert^3\Pi_- \pm1\rangle$ | $\gamma'(7 - P_2)/60$ | $-\gamma'\kappa(P_1 - P_3)/6$ | $(\gamma'/15)\mu_B B\left[\frac{g_e}{A_\Pi}(1 - 3P_2) - \frac{\eta^2}{V_1}(2 - P_2)\right]$ | $(\gamma'\kappa/30)\mu_B B[\kappa(4 - P_2) - g_e(1 - 3P_2)]$ |

[a] $\gamma' = \gamma|M|^2$.

obscure details of the structure and its magnetic-field and temperature dependencies.

Ignoring (for the moment) vibrational and librational overtones, the SO−CF model predicts four resolvable electronic bands, which we label $I = 1$−4 (in order of ascending energy) according to the right-hand side of Figure 9. Bands 1 and 2 are separated by $\Delta = V_1 - V_0$; their identification would allow $V_0$ to be estimated according to the relation

$$V_0 = (A_\Pi{}^2 - \Delta^2)/2\Delta \tag{28}$$

We start by assigning experimental bands $A_1$ and $A_2$ (Figure 1 and Table 1) to hypothetical bands 1 and 2, which gives $\Delta \approx 13$ cm$^{-1}$ and (with $A_\Pi = -33.5$ cm$^{-1}$) $V_0 \approx 38$ cm$^{-1}$. (Consequent values for the parameters $\kappa$ and $g_{||}{}^\pm$ are listed in Table 3.) The credibility of these assignments can be tested by generating spectral simulations according to[3]

$$A(E) = E\sum_{I=1}^{4}\mathbf{A}_0(I)\, f_I(E) \tag{29}$$

$$\Delta A(E) = E\sum_{I=1}^{4}[\mathbf{M}_1(I)(-\partial f_I(E)/\partial E) + (\mathbf{B}_0(I) + \mathbf{C}_0(I))\, f_I(E)] \tag{30}$$

Here, $f_I(E)$ is a normalized contour for band $I$ centered on local barycenter $\bar{E}$ $(I)$. The moment parameters have their previous meanings, except that they now refer to the individual SO−CF bands. They are obtained from Table 6 by setting $D = 0$, averaging over $\theta$, and summing the appropriate component transitions. The results are listed in Table 7.

Figures 10 and 11 show simulations obtained with $A_\Pi = -33.5$ cm$^{-1}$, $V_0 = 38$ cm$^{-1}$, and $D = 0$ cm$^{-1}$. These were generated using Gaussian contours with ad hoc bandwidths (HW$^1/e$M) of 5 cm$^{-1}$ for bands 1 and 2, and 30 cm$^{-1}$ for bands 3 and 4. $\gamma' = \gamma|M|^2$ (Table 7) was arbitrarily given a value of unity. Comparison with Figures 1 and 2 reveals general agreement with experiment. The simulated absorption (for which only the 1.6 K spectrum is presented) shows qualitatively correct dispersion for bands 1 and 2 and little temperature dependence. The *C*-term behavior of the MCD is reproduced—negative band at low energy and positive band at higher energy, with the correct temperature and field dependencies, as well as the right $\Delta A/A$ ratios. More subtly, the MCD dispersion of band 1 tends to that of an *A* term at high temperatures, and band 2 exhibits a *B* term with qualitatively correct temperature and field dependence.

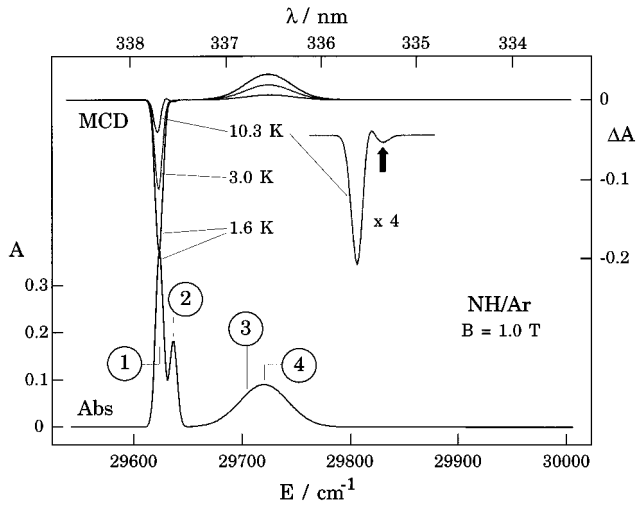


**Figure 10.** Simulated absorption spectrum ($A$; bottom) and MCD temperature dependence ($\Delta A$; top) for the $A\ ^3\Pi \leftarrow X\ ^3\Sigma^-$ system of NH/Ar, obtained using the SO−CF model with $A_\Pi = -33.5$ cm$^{-1}$ $D = 0$ cm$^{-1}$, and $V_0 = 38$ cm$^{-1}$. Gaussian band shapes were used with widths (HW$^1/e$M) of 5 cm$^{-1}$ for bands 1 and 2, and 30 cm$^{-1}$ for bands 3 and 4. The arrow in the expanded MCD spectrum at $T = 10.3$ K indicates a negative high-temperature *B* term (see text).

The last point is worthy of further comment, since *B* terms are usually regarded as being temperature independent.[3] For

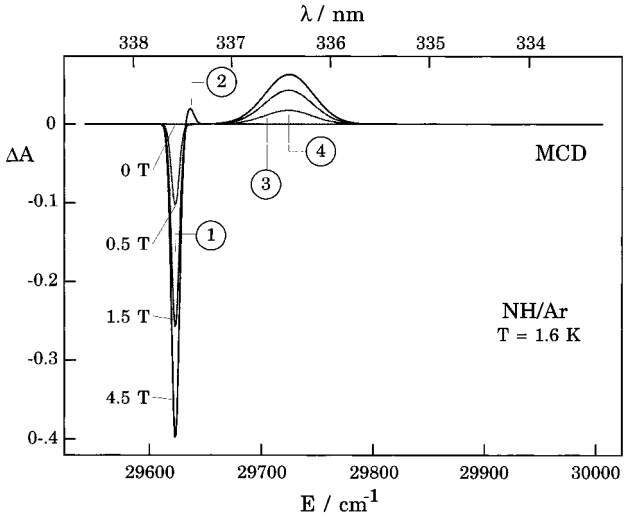


**Figure 11.** Simulated MCD magnetic-field dependence for the $A\ ^3\Pi \leftarrow X\ ^3\Sigma^-$ system of NH/Ar at $T = 1.6$ K. For further details, see the caption for Figure 10.

the hypothetical SO−CF bands, the $B$-term intensities are dependent on the populations of the ground-state Zeeman levels. This is reflected in the $\mathbf{B}_0$ expressions of Table 7 by the presence of $P_2$, the population of the central (unshifted) Zeeman level of the ground state. Consider band 2, which corresponds to a transition terminating in $|^3\Pi_-\ 0\rangle$ and whose MCD comprises $B$ terms only. This was assigned above to experimental band $A_2$, which is sharp enough for its (relatively weak) MCD to be resolved.

(i) The first term in the expression for $\mathbf{B}_0(2)$ (Table 7) arises from interactions with $\Sigma = \pm 1$ states, induced by the component of the magnetic field perpendicular to the internuclear axis. Since $A_\Pi < 0$, it represents a *positive* $B$ term whose temperature dependence is determined by the factor $(1 - 3P_2)$. In the temperature regime used in these experiments, its absolute magnitude *decreases* (with increasing $P_2$) as the temperature is raised and/or the field is lowered.

(ii) The second term in $\mathbf{B}_0(2)$ arises from interactions with $|^3\Pi_+\ 0\rangle$ induced by the magnetic-field component parallel with the internuclear axis. This corresponds to a *negative* $B$ term with temperature dependence given by $(1 + 2P_2)$. Its magnitude *increases* as the temperature is raised and/or the magnetic field is lowered.

Thus one would expect the $B$ term of band 2 to change from negative to positive as the temperature is decreased or the magnetic field is increased, which is exactly the behavior observed for band $A_2$. The high-temperature negative $B$ term is indicated in Figures 1 and 10 by an arrow in the expansions of the 10.3K MCD spectra. As the temperature is lowered and the field is increased, the $B$ term becomes more positive; at $T = 1.6$ K and $B = 4.5$ T (Figures 2 and 11), the experimental and simulated bands are again very similar.

The qualitative agreement between experimental and simulated spectra is sufficient to convince us that a CF effect *is* operating in the $A\ ^3\Pi$ term of NH/Ar. However, at a quantitative level there are significant discrepancies. First, in the simulation the positive MCD intensity is concentrated in the vicinity of experimental band $A_4$, whereas it is actually shared by bands $A_3$ and $A_4$. Second, the magnetic-field and temperature dependencies for simulated band 2 are quantitatively different from those for experimental band $A_2$. Given these problems, high precision cannot be claimed for $V_0$ or the parameters derived from it (Table 3). The conclusion that the splitting between bands $A_1$ and $A_2$ is *primarily* due to SO−CF effects seems reasonable, but it is likely that other effects (elaborated below) could perturb the energy levels and the way in which they are coupled by the magnetic field.

**3. Band Assignments.** Assignments of the structure in the spectra of NH(D)/Ar are proposed in the right-most column of Table 1. Some of these are essentially analogous to previous proposals made under the assumption of a free-rotor excited state.[19,22] For example, $A_1$ and $A_2$ are in both cases attributed to transitions terminating in the lowest states of (predominantly) $^3\Pi_2$ and $^3\Pi_1$ parentage. However, whereas the earlier workers did not explain the small $A_1-A_2$ separation in comparison with the gas phase, the present work provides a rationale in terms of CF interactions with Ar atoms. $A_1'$ is attributed to a minor metastable matrix site (see above), while $A_2'$ is assigned to a hot rotational band built on $A_1$; its shift of 25 $cm^{-1}$ (Table 1) is in close agreement with the rotational energy of $\sim$24 $cm^{-1}$ reported previously for ground-state NH/Ar.[20]

On the basis of energies alone, it is tempting to assign bands $A_3$ and $A_4$ to electronic transitions terminating in $|^3\Pi_+\ 0\rangle$ and $|^3\Pi_+\ \pm 1\rangle$ (hypothetical SO−CF bands 3 and 4). However, $A_3$ is far too intense for $^3\Pi_+\ 0 \leftarrow {}^3\Sigma^-$ and its MCD is more consistent with $^3\Pi_+\ \pm 1 \leftarrow {}^3\Sigma^-$. It therefore appears that intensity of the latter transitions is actually distributed over both $A_3$ and $A_4$. We speculate that this deviation from the predictions of the SO−CF model occurs due to perturbation of the $|^3\Pi_+\ \pm 1\rangle$ states by near coincidence with librational or phonon overtones built on lower-energy $A\ ^3\Pi$ levels. Partial support for this conjecture is provided by the ND/Ar spectra. Accidental (near) degeneracies of NH/Ar are unlikely to be reproduced for ND/Ar because of isotope shifts. Allowing for the broader bands, the spectra of ND/Ar (Figures 3 and 4) conform more closely to the simulations than do the spectra of NH/Ar; in particular, with $A_\Pi = -37.5$ $cm^{-1}$ and $V_0 = 38$ $cm^{-1}$, the separation between the MCD maximum and minimum for ND/Ar is predicted to be 106 $cm^{-1}$, which is close to the observed value of 115 $cm^{-1}$.

**4. Comparison with OH/Ar and CH/Ar.** It now remains to compare the results obtained here for the $A\ ^3\Pi$ term of NH(D)/Ar with those for the $X\ ^2\Pi$ terms of OH/Ar[1,23] and CH/Ar.[2,23]

In each case, the relevant $\pi$ orbitals are essentially nonbonding $2p_\pi$ orbitals of the non-H atom, and hence we expect the CF parameters to be similar. This is indeed the case, with $V_0$(CH/Ar) $= 39 \pm 8$ $cm^{-1}$, $V_0$(NH/Ar) $\approx 38$ $cm^{-1}$, and $V_0$(OH/Ar) $= 49 \pm 8$ $cm^{-1}$. (The CF parameter used in refs 1 and 2 is $V = 2V_0$.) There appears to be a slight trend to stronger CF with increasing atomic number, but experimental uncertainty precludes any confidence in this result.

For CH, the magnitude of the SOC constant was found to be reduced by one-third ($-11$ $cm^{-1}$) on incorporation into an Ar matrix, which we attributed to an external-atom effect due to the host matrix.[2] However, for NH and ND the changes amount to only a few percent, and they occur in opposite directions (approximately $-1$ and $+2.5$ $cm^{-1}$, respectively). Clearly the mechanism by which the matrix modifies the molecular SOC requires rethinking. It would be of interest to measure trends of $V_0$ and $A_\Pi$ for hydride radicals in matrixes of the heavier noble gases.

## V. Conclusion

The $A\ ^3\Pi \leftarrow X\ ^3\Sigma^-$ transition of NH(D) radicals trapped in solid Ar has been investigated by a combination of MCD and absorption spectroscopy. The MCD temperature dependence

reported previously by Rose[22] is confirmed. Moment analysis of the temperature and magnetic-field dependence reveals an absence of a ground-state zero-field splitting, which is consistent with free rotation in the $X\ ^3\Sigma^-$ term.[19,20] The spin−orbit parameters obtained for the $A\ ^3\Pi$ term are close to the gas-phase values, with $A_\Pi(\mathrm{NH/Ar}) = -33.5 \pm 0.3\ \mathrm{cm}^{-1}$ and $A_\Pi(\mathrm{ND/Ar}) = -37.1 \pm 1.0\ \mathrm{cm}^{-1}$.

Structural features observed in the spectra indicate that the dynamics of the radicals in the $A\ ^3\Pi$ term deviate strongly from free rotation. Interpretation and assignments of individual bands are made within a theoretical framework in which the $A\ ^3\Pi$ term is split by a spin−orbit and crystal-field interactions. A value of $V_0 \approx 38\ \mathrm{cm}^{-1}$ is proposed for the excited-state crystal-field parameter. This is consistent with values obtained previously for OH/Ar[1,23] and CH/Ar.[2,23] Simulated spectra obtained by applying the theoretical model yield semiquantitative agreement with experiment.

**Acknowledgment.** We thank Dr. Janna Rose for supplying us with earlier absorption and MCD data for NH/Ar. This research was conducted with the aid of funding from the New Zealand Lottery Grant Board, Grant GR 2224987.

## References and Notes

(1) Langford, V. S.; Williamson, B. E. *J. Phys. Chem. A* **1997**, *101*, 3119−3124.
(2) Langford, V. S.; Williamson, B. E. *J. Phys. Chem. A* **1998**, *102*, 138−145.
(3) Piepho, S. B.; Schatz, P. N. *Group Theory in Spectroscopy with Applications to Magnetic Circular Dichroism*; Wiley-Interscience: New York, 1983.
(4) Eder, J. M. *Denskschr. Wien. Akad.* **1893**, *1*, 60.
(5) Funke, G. *Z. Phys.* **1935**, *96*, 787−798.
(6) Bollmark, P.; Kopp, I.; Rydh, B. *J. Mol. Spectrosc.* **1970**, *34*, 487−499.
(7) Funke, G. *Z. Phys.* **1936**, *101*, 104−112.
(8) Dixon, R. N. *Can. J. Phys.* **1959**, *37*, 1171−1186.
(9) Veseth, L. *J. Phys. B: At. Mol. Phys.* **1972**, *5*, 229−241.
(10) Huber, K. P.; Herzberg, G. *Molecular Spectra and Molecular Structure: Constants of Diatomic Molecules*; Van Nostrand Reinhold: New York, 1979; Vol 4.
(11) Gaydon, A. G. *Spectroscopy and Combustion Theory*; Chapman and Hall Ltd: London, 1948.
(12) Smith, D. *Chem. Rev.* **1992**, *92*, 1473−1485.
(13) Schleicher, D. G.; Millis, R. L. *Astrophys. J.* **1989**, *339*, 1107−1114.
(14) Kim, S. J.; A'Hearn, M. F.; Cochran, W. D. *Icarus* **1989**, *77*, 98−108.
(15) Singh, M.; Chaturvedi, J. P. *J. P. Astrophys. Space Sci.* **1987**, *136*, 231−246.
(16) Grevesse, N.; Lambert, D. L.; Sauval, A. J.; Van Dishoeck, E. F.; Farmer, C. B.; Norton, R. H. *Astron. Astrophys.* **1990**, *231*, 225−230.
(17) Robinson, G. W.; McCarty, M. J. *J. Chem. Phys.* **1958**, *28*, 350.
(18) Robinson, G. W.; McCarty, M. J. *Can. J. Phys.* **1958**, *36*, 1590−1591.
(19) McCarty, M. J.; Robinson, G. W. *J. Am. Chem. Soc.* **1959**, *81*, 4472−4476.
(20) Bondybey, V. E.; Brus, L. E. *J. Chem. Phys.* **1975**, *63*, 794−804.
(21) Lund, P. A.; Hasan, Z.; Schatz, P. N.; Miller, J. H.; Andrews, L. *Chem. Phys. Lett.* **1982**, *91*, 437−439.
(22) Rose, J. L. Ph.D. Dissertation, University of Virginia, Charlottesville, 1987.
(23) Langford, V. S. Ph.D. Dissertation, University of Canterbury, Christchurch, 1997.
(24) Dunford, C. L.; Williamson, B. E. *J. Phys. Chem. A* **1997**, *101*, 2050−2054.
(25) Dunford, C. L. Ph.D. Dissertation, University of Canterbury, Christchurch, 1997.
(26) Buckingham, A. D.; Stephens, P. J. *Annu. Rev. Phys. Chem.* **1966**, *17*, 399−432.
(27) Herzberg, G. *Molecular Spectra and Molecular Structure: Spectra of Diatomic Molecules*, 2nd ed.; Van Nostrand Reinhold: New York, 1950; Vol. 1.
(28) Wayne, F. D.; Radford, H. E. *Mol. Phys.* **1976**, *32*, 1407−1422.
(29) Hougen, J. T. *Natl. Bur. Stand. (U.S.) Monogr.* **1970**, *115*.
(30) Williamson, B. E.; Roser, D. C.; Vala, M. *J. Phys. Chem.* **1994**, *98*, 3624−3630.